Acta Oceanol. Sin., 2021, Vol. 40, No. 6, P. 16–25
https://doi.org/10.1007/s13131-021-1786-2
http://www.aosocean.com
E-mail: ocean2@hyxb.org.cn

Utilizing $^{234}Th/^{238}U$ disequilibrium to constrain particle dynamics in hydrothermal plumes in the Southwest Indian Ocean

Weifeng Yang[1, 2*], Xinxing Zhang[3], Min Chen[2], Ziming Fang[4], Yusheng Qiu[2]

[1] State Key Laboratory of Marine Environmental Science, Xiamen University, Xiamen 361102, China

[2] College of Ocean and Earth Sciences, Xiamen University, Xiamen 361102, China

[3] North China Sea Environmental Monitoring Center, State Oceanic Administration, Qingdao 266033, China

[4] Department of Ocean Science, Hong Kong University of Science and Technology, Hong Kong 999077, China

Received 19 February 2020; accepted 4 June 2020

Abstract

Metal-enriched minerals have been widely observed near hydrothermal vent fields. However, the dynamics of particulate metals influenced by hydrothermal activities is poorly constrained. Here, radioactive ^{234}Th in both dissolved and particulate phases were used to examine the kinetics of particle-reactive metal adsorption, removal, and residence in a newly found hydrothermal plume over the Southwest Indian Ridge. The results showed a relatively low value on $^{234}Th/^{238}U$ ratios (i.e., 0.73–0.88) compared to the deep oceans, indicating an enhanced adsorption of particle-reactive metals onto particulate matter in the plume. Based on the ^{234}Th-^{238}U disequilibria, the adsorption and sinking rate constants of ^{234}Th averaged (0.009±0.001) d^{-1} and (0.113±0.024) d^{-1} in the hydrothermal plume, corresponding to the residence times of (115±19) d and (16±5) d for dissolved and particulate ^{234}Th, respectively. This timescale allows vent-discharged particle-reactive metals to disperse hundreds to thousands of miles away. Thus, hydrothermal activities might influence the metal distribution in deep ocean over a very large scope. Also, a high sinking flux of (36.2±5.4) Bq/(m^2·d) for ^{234}Th was observed for the plume, suggesting an enrichment of metal in particles deposited close to the vent. The enhancement of particle sinking could also benefit the transport of organic carbon and nitrogen and fuel the benthic ecosystems under the plume regimes. Thus, hydrothermal plumes may have an impact on both the elemental geochemistry and/or ecosystem to the deep oceans interior than previous expectation.

Key words: thorium-234, particle dynamics, hydrothermal plume, Indian Ocean

Citation: Yang Weifeng, Zhang Xinxing, Chen Min, Fang Ziming, Qiu Yusheng. 2021. Utilizing $^{234}Th/^{238}U$ disequilibrium to constrain particle dynamics in hydrothermal plumes in the Southwest Indian Ocean. Acta Oceanologica Sinica, 40(6): 16–25, doi: 10.1007/s13131-021-1786-2

1 Introduction

Hydrothermal events emit a large amount of hot fluid with metal elements into seawater (Ingebritsen and Evans, 2019). These metals precipitate by forming polymetallic sulfides (Ray et al., 2018) which will effectively absorb many other metals (e.g., Pb, Po, Th, Zn) (Liao et al., 2017; Pavia et al., 2019), phosphorus (Kadko et al., 1994), carbon and nitrogen (Toner et al., 2009) from ambient seawater. Metal-enriched particles are utilized by filter-feeders, resulting in an evident metal-accumulation, such as Hg, Cu, Pb, Cr, Ni and Zn, in mollusks which habited around the hydrothermal vents (Peng et al., 2011; Pancaldi et al., 2019). Hence, metal cycling in hydrothermal systems and similar submarine volcanic eruption (Lozano-Bilbao et al., 2018) have attracted extensive attentions according to their influences in associated ecosystem (Chakraborty et al., 2014). However, the influencing scope of the hydrothermal activities in deep ocean is difficult to define, due to the lack of technologies to constrain the resident timescale and the dispersal range of the metals (Yang et al., 2016).

Sediment trap is frequently used for particle collection directly from the upper ocean (Hung and Gong, 2010; Hung et al., 2012) or the deep water (Ran et al., 2015; Zhang et al., 2019). It can provide valuable information on sinking flux of the real sinking particles (Shih et al., 2019). In hydrothermal systems close to the vents, sediment traps have also been used to quantify the particle flux and to collect sulfides which could be used to characterize particle composition (German et al., 2002; Beaulieu et al., 2009). Hydrothermal plumes usually cover a large spatial scope and may vary spatiotemporally with the deep currents. Using sediment traps to track particle cycling in the hydrothermal plumes would cost high.

Radiogenic ^{234}Th ($T_{1/2}$=24.1 d) is a tool for constraining the adsorption, sinking and resident timescales of elements in the upper ocean (Bi et al., 2013; Huang et al., 2013; Pavia et al., 2019). Since its particle-reactive nature in seawater (Lin et al., 2014) similar to some other metals (e.g., Pb, Po) (Boisson et al., 2001) and phosphorus (Kadko et al., 1994; Lin et al., 2012), ^{234}Th is readily absorbed onto particulate matter and settles downwards (Buesseler et al., 1992; Yang et al., 2016). Thus, ^{234}Th has been determined and used in the upper oceans especially in the euphotic zone to constrain biogenic carbon sinking to the ocean interior

Foundation item: The National Natural Science Foundation of China under contract Nos 41721005 and 41476061; China Ocean Mineral Resources R&D Association Programs under contract Nos DY135-E2-2-03 and DY125-22-QY-17; the Fundamental Research Funds for the Central Universities under contract No. 20720190102.
*Corresponding author, E-mail: wyang@xmu.edu.cn

(i.e., the biological pump) (Ma et al., 2011). In deep oceans, the total ^{234}Th is often found to be in equilibrium with its parent ^{238}U (Benitez-Nelson et al., 2001a; Coppola et al., 2005; Anand et al., 2018) due to scarce particles and long residence time of ^{234}Th. This observation seems to disable ^{234}Th to trace the kinetics of element adsorption in deep oceans. However, previous studies reveal that ^{234}Th in hydrothermal plumes is deficit, to a varying degree, with respect to ^{238}U (Kadko et al., 1994; Owens et al., 2015; Pavia et al., 2019), ascribing to the abundant hydrothermal particles and enhanced metal adsorption. Therefore, ^{234}Th-^{238}U disequilibrium could be an efficient technique to constrain the resident timescales and dispersal range of particle-reactive metals emitted from the hydrothermal vents.

Recently, hydrothermal plumes at different depths from active vents were confirmed over the ultraslow-spreading Southwest Indian Ocean Ridge (SWIR) by the distributions of Fe, Mn, particulate content anomaly and zinc sulfide (Sun, 2011; Wang et al., 2012; Sun et al., 2014). These findings provide an opportunity for us to examine the influential scope of hydrothermal fluids and the residence and dispersal of metals along the plume. In this study, ^{234}Th was determined in an identified hydrothermal plume over the SWIR in order to (1) compare the difference in radioactive ^{234}Th contents between hydrothermal plume and general deep oceans; (2) quantify the resident timescale and the adsorption behavior of particle-associated metals; and (3) preliminarily evaluate the influence of hydrothermal plume on deep ocean carbon cycling and its environmental implications.

2 Materials and methods

2.1 *Sampling*

Sampling station CTD3 is located right over the ultraslow-spreading SWIR with a water depth of about 1 800 m (Fig. 1). Within 1 000–1 600 m, elevated suspended particulate matter (SPM) contents comparing with the overlying water column and the existence of zinc sulfide (ZnS) mineral during the same cruise (Sun, 2011; Sun et al., 2014) identified the hydrothermal effluent plume from three active vents on the SWIR (Tao et al., 2012).

Seawater and SPM were collected onboard the R/V *Dayang I* during the DY115-21 cruise in February 2010. The contents of SPM were quantified through the difference in the weight between dried particles at 40°C and wet particles (Sun, 2011). In total, thirteen depths (i.e., 3 m, 50 m, 100 m, 280 m, 300 m, 500 m, 800 m, 1 000 m, 1 400 m, 1 450 m, 1 500 m, 1 550 m, and 1 600 m) were occupied for ^{234}Th determination. Below 1 200 m, SPM contents indicated evident hydrothermal plume signals (Fig. 2, Sun et al., 2014), thus high-resolution sampling with 50 m intervals was conducted to collect typical plume information. In the euphotic zone (0–100 m), ^{234}Th was also sampled to examine the difference between the surface ocean and the hydrothermal plume by comparing their characteristics.

2.2 *^{234}Th determination*

At each specific depth, about 8 L of seawater were filtered through a quartz fiber membrane (combusted at 450°C for 4 h) with 1 μm pore size (QMA, Whatman) to collect particles for particulate ^{234}Th (i.e., $^{234}Th_p$) measurement. Particle-contained membranes were dried at 60°C immediately and counted using a low-level beta counter with the counting efficiency of 41% (Yang et al., 2016) until the net counting errors were less than ±6%. A second counting was conducted after 150 d for quantifying other beta emitters in order to remove their contribution to the first obtained ^{234}Th counts.

Dissolved ^{234}Th (i.e., $^{234}Th_D$) was concentrated from 4 L of filtrate using the small-volume method (Benitez-Nelson et al., 2001b). In brief, the pH value of filtrate was adjusted to 9.0 using ammonium hydroxide, then $KMnO_4$ and $MnCl_2$ solution were added to form MnO_2 particle. After 6 h, MnO_2 precipitate was separated from solution via filtration using QMA membrane. The recovery was 95.7%±1.0% (mean±SD, n=5) (Yang et al., 2015a). After dried at 60°C, dissolved ^{234}Th activity was measured by the low-level beta counter in a manner similar to particulate ^{234}Th but with ±1σ counting error. The concentrations of both dissolved and particulate ^{234}Th were calculated based on the two

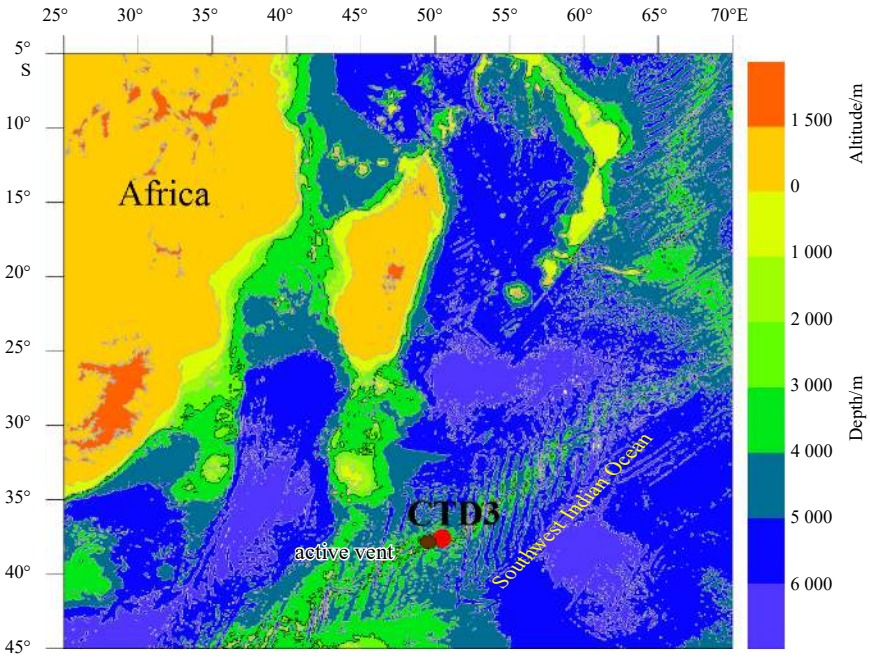

Fig. 1. Sampling location over the Southwest Indian Ocean Ridge.

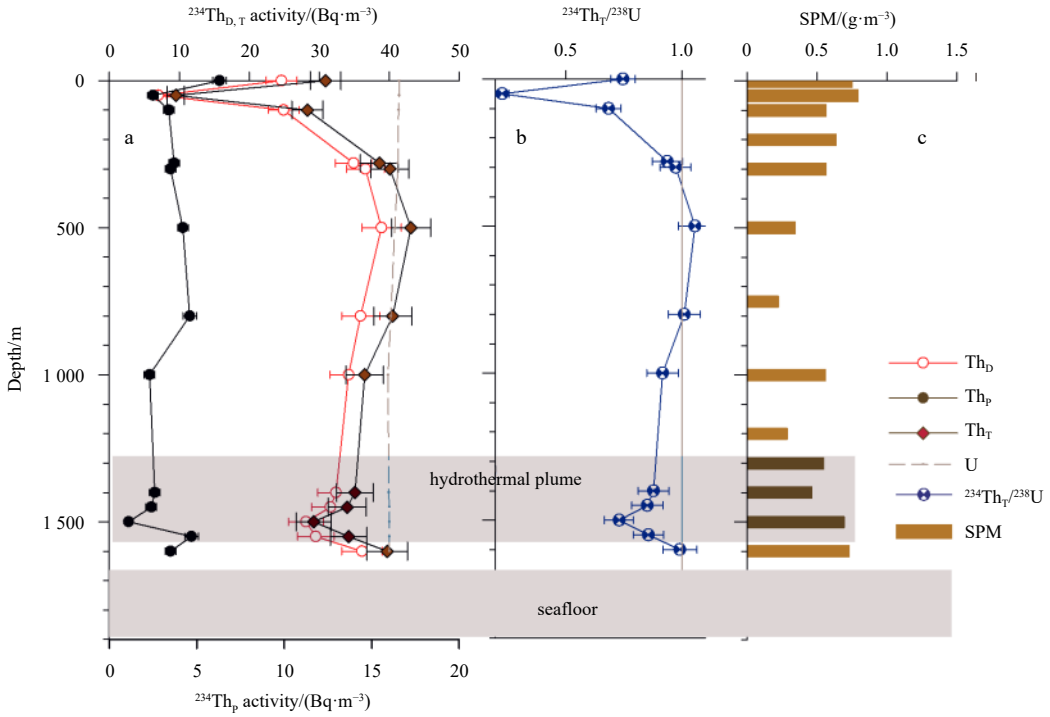

Fig. 2. Vertical distributions of dissolved, particulate and total ^{234}Th concentrations (a), $^{234}Th_T/^{238}U$ ratios (b) and suspended particulate matter (SPM) concentrations (c). SPM data are obtained from Sun (2011) at the same station.

measurements and corrected for recovery, blank counts, and sampling time. The total ^{238}U activities were calculated using the newly updated ^{238}U-salinity relationship (Owens et al., 2011). The uncertainties of dissolved and particulate ^{234}Th measurement were propagated from the counting errors. The total ^{234}Th and ^{234}Th/^{238}U ratio uncertainties were propagated from dissolved and particulate ^{234}Th.

2.3 *Calculations of kinetic parameters of ^{234}Th and POC fluxes*

In the oceans, adsorption and sinking of particle-reactive radionuclides (e.g., ^{234}Th, ^{210}Pb and ^{210}Po) were following the first-order reaction kinetics (Bacon et al., 1976; Buesseler et al., 1992). Thus, the adsorption and sinking of ^{234}Th in both euphotic zone and hydrothermal plume were expressed as follows:

$$\frac{dA_{ThD}}{dt} = \lambda A_U - \lambda A_{ThD} - kA_{ThD}, \quad (1)$$

$$\frac{dA_{ThP}}{dt} = kA_{ThD} - \lambda A_{ThP} - \varphi A_{ThP}, \quad (2)$$

where A_{ThD}, A_{ThP}, and A_U are the activities of $^{234}Th_D$, $^{234}Th_P$, and ^{238}U (Bq/m^3); λ is the decay constant of ^{234}Th (0.029 d^{-1}), k represents the adsorption rate constant (d^{-1}). Hence, λA_U reflects the generation rate of $^{234}Th_D$ via ^{238}U decay (Bq/(m^3·d)). λA_{ThD} and λA_{ThP} represent the decay terms of dissolved and particulate ^{234}Th. kA_{ThD} is the adsorption rate of $^{234}Th_D$. φ is the sinking rate constant of $^{234}Th_P$ (d^{-1}). φA_{ThP} denotes the sinking rate of $^{234}Th_P$. The residence times of dissolved and particulate ^{234}Th are calculated from the reciprocals of adsorption and sinking rate constants (d). At the steady-state, the adsorption, sinking rate constants and residence times of ^{234}Th can be calculated, as well as the adsorption and sinking rates.

The active particle dynamics in the hydrothermal plume over the SWIR suggest that particulate matter and its combined metals would quickly settle to bottom water and seafloor, and consequently shape different environment regions from general deep oceans (Yang et al., 2016). This study attempt to reveal the characteristics of particulate components sinking using limited data based upon the widely used flux calculation (Buesseler et al., 1992):

$$F_{absorb} = \lambda \left(\int_{1\,400}^{1\,600} A_U dz - \int_{1\,400}^{1\,600} A_{ThD} dz \right), \quad (3)$$

$$F_{sinking} = \lambda \left(\int_{1\,400}^{1\,600} A_U dz - \int_{1\,400}^{1\,600} A_{ThT} dz \right), \quad (4)$$

where F_{absorb} and $F_{sinking}$ are the adsorption and sinking fluxes of ^{234}Th (Bq/(m^2·d)), respectively; $\int_{1\,400}^{1\,600} A_U dz$, $\int_{1\,400}^{1\,600} A_{ThD} dz$ and $\int_{1\,400}^{1\,600} A_{ThT} dz$ represent the total amounts of ^{238}U, $^{234}Th_D$, and the total ^{234}Th (i.e., $^{234}Th_T$) (Bq/m^2) in the hydrothermal plume (1 400–1 600 m).

The sinking fluxes of SPM, POC and PON were calculated through the proposed equation (Buesseler et al., 1992; Yang et al., 2016):

$$F_{i,sinking} = F_{Th,sinking} \times \frac{i}{A_{ThP}}, \quad (5)$$

where $F_{i,sinking}$ represents the fluxes of SPM, POC and PON, and i denotes the contents of SPM, POC and PON.

3 Results

In surface euphotic water (0–100 m), the total ^{234}Th concentrations ranged from 9.5 Bq/m^3 to 30.8 Bq/m^3 with an average of (22.8±3.3) Bq/m^3 (Fig. 2). The averaged $^{234}Th_T/^{238}U$ ratios was 0.55±0.08, corresponding to a typical deficit of ^{234}Th with respect to ^{238}U in the upper water of Indian Ocean (Yang et al., 2016; Anand et al., 2018). The lowest $^{234}Th_T$ value was found at depth 50 m, matching with the highest SPM content in the euphotic zone. In the twilight zone (i.e., 100–1 000 m), $^{234}Th_T$ activity was overall equal to ^{238}U activity (Fig. 2) with the $^{234}Th_T/^{238}U$ ratios ranged from 0.92 to 1.06 (avg. 0.98±0.04), showing an equilibrium feature as widely observed in the mesopelagic in the Indian and Atlantic sectors of the Southern Ocean (Coppola et al., 2005; Roca-Martí et al., 2017), Pacific Ocean (Charette et al., 1999; Buesseler et al., 2009) and Atlantic Ocean (Owens et al., 2015). It is notable that $^{234}Th_T$ activity showed lower value than ^{238}U activity between 1 400 m and 1 550 m below the twilight zone, ranging from 28.7 Bq/m^3 to 35.0 Bq/m^3 and averaging 33.2 Bq/m^3. Therefore, the $^{234}Th_T/^{238}U$ ratios varied from 0.73 to 0.88 with an average of 0.83±0.04, contrasting with the usual equilibria between ^{234}Th and ^{238}U observed in bathypelagic waters, e.g., the North Pacific Subtropical Gyre (Benitez-Nelson et al., 2001a), the Northeast Atlantic (Schmidt, 2006), and the northern Indian Ocean (Anand et al., 2018).

Overall, the deficit extents of the total ^{234}Th mirror the vertical distribution of SPM (data from Sun, 2011) in the water column over the SWIR (Fig. 2c). In the upper 200 m, low $^{234}Th_T/^{238}U$ ratios (^{234}Th deficit) correspond to high SPM contents, indicating the predominant role of particles in absorbing and removing ^{234}Th. Within 280–800 m depth, SPM showed low concentrations and matched with a weak removal of ^{234}Th and around 1.0 of $^{234}Th_T/^{238}U$ ratios (Fig. 2c). At 1 000 m, high SPM contents were also observed with a slightly low $^{234}Th_T/^{238}U$ ratio. Below 1 200 m, the low $^{234}Th_T/^{238}U$ ratios and high SPM were simultaneously observed.

4 Discussion

4.1 *Unusually low ^{234}Th in the hydrothermal plume vs. normal deep water*

In normal bathypelagic zone (1 000–4 000 m), available data suggest that ^{234}Th is often comparable to ^{238}U (Benitez-Nelson et al., 2001a; Coppola et al., 2005; Anand et al., 2018) due to scarce SPM and weak ^{234}Th removal, which allow ^{234}Th to reach equilibrium with ^{238}U as observed in the mesopelagic at the study site (Fig. 2b). However, ^{234}Th showed significant deficit with respect to ^{238}U within the hydrothermal effluent plume (below 1 200 m) over the SWIR (Fig. 2b), indicating an effective removal of ^{234}Th. In seawater, ^{234}Th removal includes sinking with particles after adsorption (Yang et al., 2015a) and *in situ* decay. In oceanic settings with abundant particulate matter, for example in the productive euphotic zone and turbid benthic nepheloid layer (BNL), adsorption and sinking usually dominate ^{234}Th removal and result in ^{234}Th deficit (Rutgers van der Loeff et al., 2002; Bacon and Rutgers van der Loeff, 1989; Turnewitsch et al., 2008). In environments with less contents of particles, decay often dominates ^{234}Th removal and leads to the equilibria between ^{234}Th and ^{238}U as observed in general bathypelagic water (Anand et al., 2018). Thus, the abnormal ^{234}Th deficit is attributed to the enhanced ^{234}Th removal via particle settling in the hydrothermal plume. In fact, a recent study observed intensive removal of thorium isotopes (i.e., ^{234}Th, ^{230}Th) in a hydrothermal plume (Hayes et al., 2015). As shown in Fig. 3, the $^{234}Th_T/^{238}U$ ratio decreases with elevated SPM concentration, supporting the effective removal of ^{234}Th through on particulate matter in the studied hydrothermal plume.

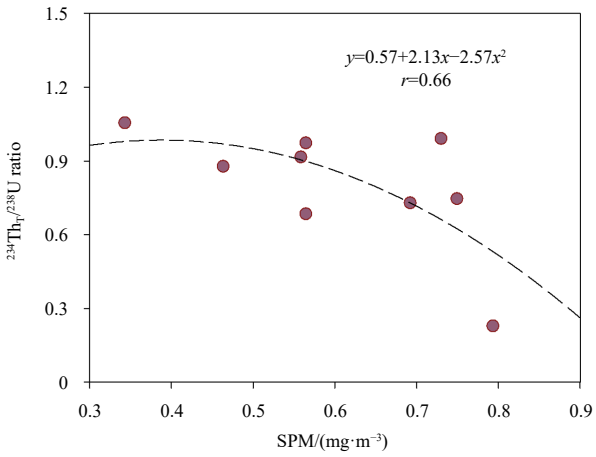

Fig. 3. Relationship between the $^{234}Th_T/^{238}U$ ratio and SPM content.

Unlike the euphotic zone, less abundance of phytoplankton was found in the hydrothermal plume. Hence, particles in plume was less influenced by biogenic origin. Results showed that the elevated particles are mainly as sulfide minerals in the hydrothermal plume from the current study (Sun, 2011; Sun et al., 2014). Since absorption natures of sulfides were different from biogenic particles (i.e., particulate organic matter, biogenic silica, and bio-carbonate), they might show distinguishable affinity with ^{234}Th. Indeed, the distribution coefficients (K_d) of ^{234}Th in the photic zone (from 1.70×10^5 L/kg to 4.52×10^5 L/kg) were higher than 0.55×10^5–1.75×10^5 L/kg in the hydrothermal plume (Fig. 4), implying a weak affinity of sulfide minerals for ^{234}Th comparable with biogenic particulate. Previous studies indicated that a strong affinity of organic matter with ^{234}Th, followed by Mn- and Fe-oxides and carbonate, biogenic silica (Guo et al., 2002; Yang et al., 2009). While Hayes et al. (2015) reported that the K_d values of ^{230}Th on Fe/Mn (hydr)oxides were 1–2 orders of magnitude greater than those for organic matter. Enriched Fe and Mn were reported in the hydrothermal plume over the SWIR (Wang et al., 2012), Fe- and Mn-contained sulfides seem not to be effective in removing ^{234}Th as biogenic particles, probably due to their sulfide forms (Sun et al., 2014). This view is corroborated by the comparable SPM concentrations between the photic zone and hydrothermal plume (Fig. 2c) but lower K_d values of ^{234}Th in the plume (Fig. 4).

Like ^{234}Th, particle-reactive elements such as Pb, Po, and P are easy to be absorbed by particulate matter in seawater (Feely et al., 1990; Yang et al., 2013, 2015b) and then sink to seafloor (Boisson et al., 2001; Ma et al., 2017). The enhanced ^{234}Th removal (Fig. 2) indicated that hydrothermal plume is a special oceanic setting characterized by active particle dynamics. Many metals from the hydrothermal effluent would settle down to seafloor below the plume, which might increase the metal accumulation in benthic mollusks (Kádár et al., 2007). Indeed, the available study indicated increased Pb flux in the hydrothermal vent area (Boisson et al., 2001). Thus, given particle-reactive metals, their accumulation in organisms in the hydrothermal plume was probably different from the general aphotic deep ocean, intensive investigation was needed before polymetallic sulfides mining.

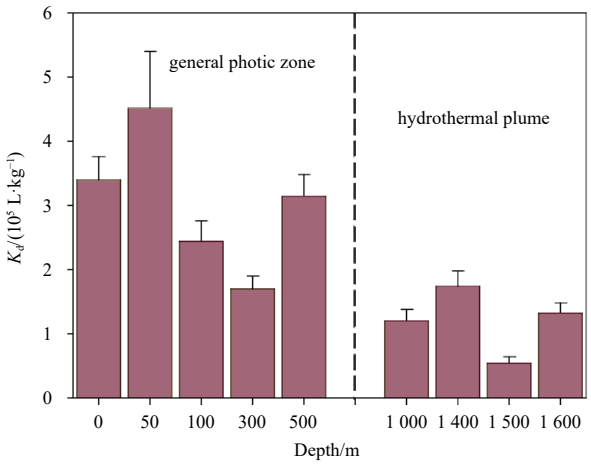

Fig. 4. Contrasting distribution coefficients of ^{234}Th between general photic waters (i.e., euphotic and twilight water) and hydrothermal plume.

4.2 *Radioactive ^{234}Th adsorption and sinking in the hydrothermal plume*

Thermodynamically, distribution coefficients illustrated the difference in the adsorption of ^{234}Th on particulate matter between the euphotic zone and hydrothermal plume (Fig. 4). Here, this study also attempt to examine the possible differences in the kinetics during ^{234}Th adsorption and sinking in the two different types of oceanic environments.

In the hydrothermal plume, the adsorption constants varied from 0.007 d^{-1} to 0.012 d^{-1} with an average of (0.009±0.001) d^{-1} (Fig. 5), comparable to (0.010±0.002) d^{-1} (ranging from 0.008 d^{-1} to 0.012 d^{-1}) in another hydrothermal plume within 2 000–3 100 m over the SWIR (Yang et al., 2016). However, these constants were much lower than (0.060±0.008) d^{-1} (from 0.019 d^{-1} to 0.142 d^{-1}) in the euphotic zone (Table 1), indicating that sulfides in the hydrothermal plume need longer time to absorb ^{234}Th than biogenic particles in the euphotic zone. In fact, the residence times of dissolved ^{234}Th varied from 82 d to 150 d with an average of (115±19) d (Table 1). By contrast, they showed a range of 7–52 d, averaging (37±4) d in the euphotic zone. Obviously, approximately 3 fold higher residence time supported the slow transfer of ^{234}Th from dissolved form to particulate phase in the hydrothermal plume. Although only a few studies have been reported the residence times of ^{234}Th in hydrothermal plumes, the results were consistent with the reported values. Yang et al. (2016) reported (108±19) d in a hydrothermal plume versus (60±22) d in the euphotic zone over the SWIR. In addition, Kadko et al. (1994) showed dissolved ^{234}Th residence time of 18–102 d over the North Cleft segment of the Juan de Fuca Ridge. Owens et al. (2015) presented the mean residence time of 100 d in the Trans-Atlantic Geotraverse (TAG) hydrothermal plume. Pavia et al. (2019) reported the adsorption constants of 0.003 d^{-1} to 0.008 d^{-1}, corresponding to 122–302 d in a hydrothermal plume over the Southeast Pacific Ocean Ridge. These available data suggested that particle-reactive metals seem to reside over tens of days in the hydrothermal plumes. Such a timescale allows particle-reactive metals, either emitted from hydrothermal vents or captured from ambient seawater during plume dispersal, to spread over a large spatial scale and the bathypelagic environments could be influenced extensively.

In the hydrothermal plume, the sinking rate constants of $^{234}Th_P$ spanned an order of magnitude, varying from 0.020 d^{-1} to 0.291 d^{-1} (Fig. 5) and averaging (0.113±0.024) d^{-1} (Table 1). These constants correspond to 3–29 d residence times (avg. (16±5) d). In another hydrothermal plume over the SWIR, the sinking rate constants varied from 0.031 d^{-1} to 0.121 d^{-1} and the residence times from 8 d to 32 d (Yang et al., 2016), comparable to the results of this study. In the euphotic zone, $^{234}Th_P$ showed comparable sinking rate constants (from 0.048 d^{-1} to 0.367 d^{-1}, avg. (0.175±0.016) d^{-1}) and residence times (3–21 d, avg. (11±2) d) (Table 1). It is clear that particles in the hydrothermal plume seemed to settle as fast as biogenic particulate did in the euphotic zone though their adsorption constants had 6-fold difference (Table 1). In addition, the sinking constants of ^{234}Th were an order of magnitude higher than its adsorption constants (Table 1), indicating an effective sinking. Thus, hydrothermal particles probably play important role in transporting particle-reactive metals from deep seawater to sediment over the SWIR. Unlike the observation of this study, $^{234}Th_P$ appeared to reside for longer time (>150 d) in the hydrothermal plumes over the Juan de Fuca Ridge and the TAG field (Kadko et al., 1994; Owens et al., 2015). This difference may result from a close distance from the sampling site to the active hydrothermal vents (Tao et al., 2012).

The adsorption rate of $^{234}Th_D$ varied from 0.215 Bq/(m^3·d) to 0.342 Bq/(m^3·d) with an average of (0.275±0.022) Bq/(m^3·d) (Table 1), comparable to (0.292±0.042) Bq/(m^3·d) in another plume over the SWIR (Yang et al., 2016) and 0.300 Bq/(m^3·d) at the TAG (Owens et al., 2015). However, these rates were lower than 0.295–0.783 Bq/(m^3·d) estimated using dataset over the Juan de Fuca Ridge (Kadko et al., 1994). The sinking rate of $^{234}Th_P$ ranged from 0.140 Bq/(m^3·d) to 0.310 Bq/(m^3·d) and averaged (0.197±0.022) Bq/(m^3·d) (Fig. 5d), which was the same as observations in adjacent hydrothermal plume within 2 900–3 100 m over the SWIR (from 0.130 Bq/(m^3·d) to 0.287 Bq/(m^3·d), avg. (0.197±0.042) Bq/(m^3·d) (Yang et al., 2016). Thus, it seems that the adsorption and sinking rates of ^{234}Th have similar characteristics in hydrothermal plumes at different sites over the SWIR (Table 1; Yang et al., 2016) though they were different from those in the Pacific Ocean (Kadko et al., 1994). This difference indicated the different particle kinetics in terms of various hydrothermal plumes, probably due to the different composition of the hydrothermal particle from different vents.

4.3 *The enhancement of ^{234}Th and other particulate components sinking*

The adsorption flux of ^{234}Th was (52.4±5.4) Bq/(m^2·d) in the hydrothermal plume, which was comparable to available ^{234}Th adsorption flux in the plume over the SWIR ((46.0±5.6) Bq/(m^2·d); Yang et al., 2016), at the TAG (45.4 Bq/(m^2·d); Owens et al., 2015), but lower than 44.3 Bq/(m^2·d) to 129.7 Bq/(m^2·d) at the Juan de Fuca Ridge (Kadko et al., 1994). The sinking flux of ^{234}Th was (36.2±5.4) Bq/(m^2·d) at the study site, which was much higher than 16.0 Bq/(m^2·d) reported for another SWIR plume (Yang et al., 2016). Combining with all the kinetic parameters (i.e., rate constant, rate, flux and residence time), it appeared that similar characteristics of the hydrothermal plume were seen over the ultraslow-spreading SWIR to TAG and large difference from the Juan de Fuca Ridge.

In addition to particle-reactive metals, the cycling of some particle components (e.g., SPM, nitrogen and carbon) could change with the hydrothermal plumes. Previous studies reported that particles have the capability to disperse hundreds of kilometers with the hydrothermal plumes (Siegel et al., 2008; Wang et al., 2012; Estapa et al., 2015). Based on a preliminary estimation

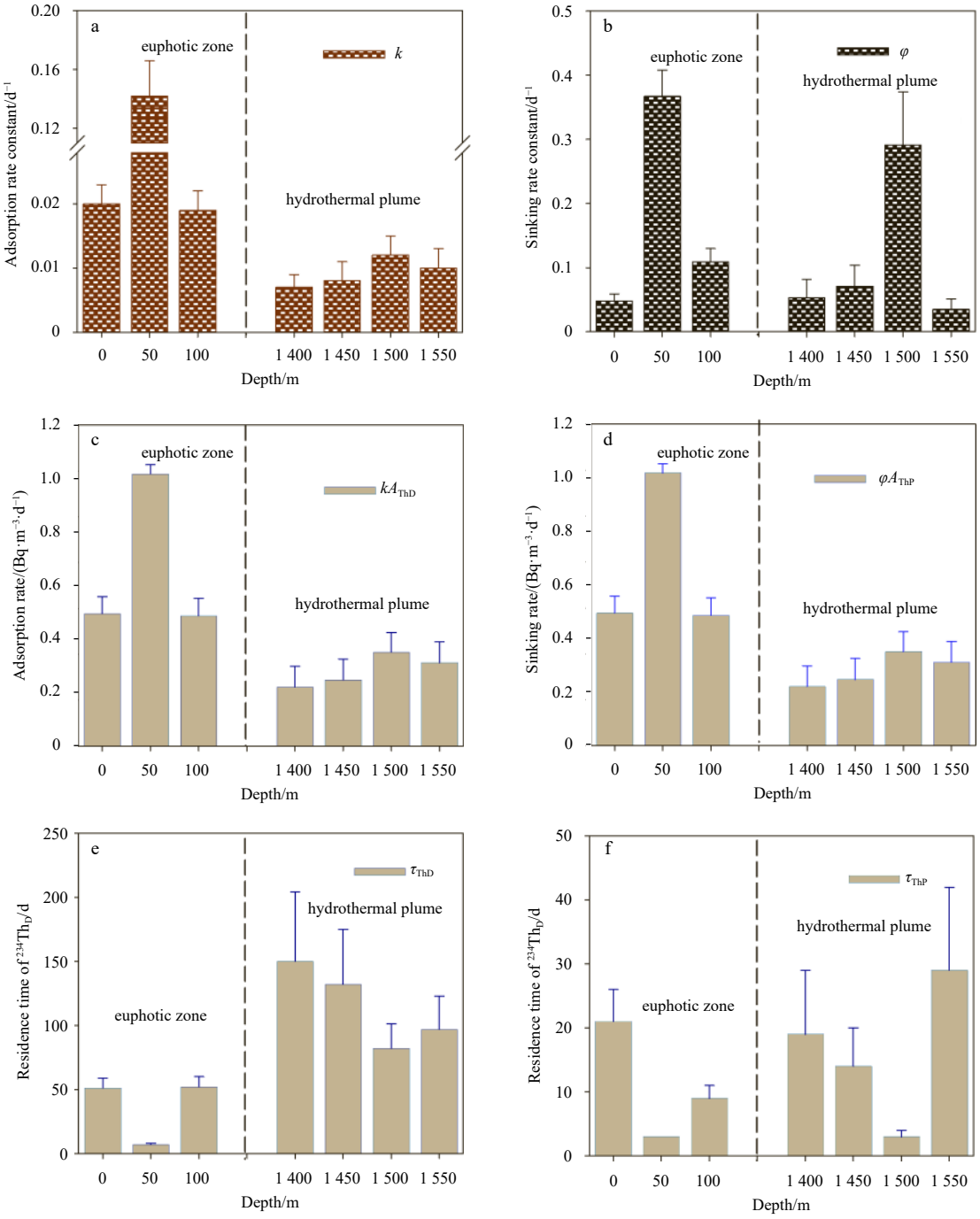

Fig. 5. Comparisons of adsorption constant (a), removal constant (b), adsorption rate (c), removal rate (d) of ^{234}Th, residence times of dissolved (e) and particulate (f) ^{234}Th between the euphotic zone and hydrothermal plume.

using Eq. (5), the sinking flux of SPM out of the plume reached (7.5±1.3) g/(m²·d). This magnitude is comparable to the cross-shelf process induced high particle flux in the mesopelagic South China Sea (Ma et al., 2017), indicating the crucial role of hydrothermal plume in affecting the particle cycling in the ocean interior. Hydrothermal particles usually contain abundant Fe and Mn compounds (Sun et al., 2014), which were expected to induce DOC aggregation in the hydrothermal plumes (Toner et al., 2009) and POC could be effectively delivered to sediments (German et al., 2015). The only available high POC sinking flux from a hydrothermal plume also supports these views (Yang et al., 2016). In order to evaluate the role of the studied hydrothermal plume in affecting carbon and nitrogen cycling, this study conservatively adopt the minimum POC and PON values reported in an adjacent plume (Yang et al., 2016), i.e., 0.72 μmol/L (in terms of carbon) and 0.17 μmol/L (in terms of nitrogen). The calculated POC and PON fluxes were (7.4±1.3) mmol/(m²·d) (in terms of carbon) and (1.8±0.3) mmol/(m²·d) (in terms of nitrogen), respectively. These values seem to be comparable with reported values of (9.3±0.6) mmol/(m²·d) (in terms of carbon) and (2.2±0.6) mmol/(m²·d) (in terms of nitrogen) from another hydrothermal plume over the SWIR (Yang et al., 2016). The POC flux was much higher

Table 1. Adsorption (k) and removal constants (φ) of ^{234}Th, adsorption (kA_{ThD}) and removal rates (φA_{ThP}) in the euphotic zone and hydrothermal plume, residence times of dissolved and particulate ^{234}Th (τ_{ThD}, τ_{ThP})

Zone	Depth/m	k/d^{-1}	φ/d^{-1}	kA_{ThD}/(Bq·m^{-3}·d^{-1})	φA_{ThP}/(Bq·m^{-3}·d^{-1})	τ_{ThD}/d	τ_{ThP}/d
Euphotic zone	0	0.020±0.003	0.048±0.011	0.482±0.062	0.302±0.063	51±8	21±5
	50	0.142±0.024	0.367±0.041	0.989±0.033	0.917±0.034	7±1	3±0
	100	0.019±0.003	0.109±0.021	0.474±0.063	0.375±0.064	52±8	9±2
	mean	0.060±0.008	0.175±0.016	0.649±0.031	0.531±0.032	37±4	115±19
Hydrothermal plume	1 400	0.007±0.002	0.020±0.021	0.216±0.075	0.140±0.076	150±54	19±10
	1 450	0.008±0.003	0.071±0.033	0.240±0.077	0.171±0.077	132±43	14±6
	1 500	0.012±0.003	0.291±0.083	0.342±0.072	0.311±0.073	82±19	3±1
	1 550	0.010±0.003	0.035±0.016	0.303±0.075	0.166±0.076	97±26	29±13
	mean	0.009±0.001	0.113±0.024	0.275±0.037	0.197±0.038	11±2	16±5

than those of <2 mmol/(m^2·d) (in terms of carbon) observed at 2 000 m (Rixen et al., 2019) and comparable to the maximal POC flux (9.0 mmol/(m^2·d) (in terms of carbon)) out of the euphotic zone in the northern Indian Ocean (Anand et al., 2018), indicating other POC contribution in addition to the surface ocean to the hydrothermal plumes. Also, the POC flux in our study was even higher than that of <6 mmol/(m^2·d) (in terms of carbon) observed at 100–2 000 m in the South China Sea where was identified by cross-shelf lateral particle transport (Shih et al., 2019), indicating the significant influence of hydrothermal plume on POC sinking in deep oceans. The POC flux was calculated using the POC/^{234}Th$_p$ ratio on SPM collected by bottle sampler. Earlier research speculated that large particles (>53 μm) represent the sinking POC (Coppola et al., 2002). Recently, some studies found small size particles accounted for a major fraction of the sinking particles in the open oceans (Hung and Gong, 2010; Hung et al., 2012). Since the POC/^{234}Th$_p$ ratio sometimes varied with particle size (Hung et al., 2012), it is difficult to validate the specific size of representing the sinking POC currently. Bottle-collected particles might represent the upper limit of POC flux (Cai et al., 2008). Thus, this study's estimates may constrain the maximal POC flux out of the studied plume. POC flux is usually less than 2 mmol/(m^2·d) (in terms of carbon) in the general deep ocean (Smith and Rabouille, 2002; Ran et al., 2015). Obviously, POC and PON fluxes to the seafloor was increased by the hydrothermal plumes. Together with the radioactive ^{234}Th flux, high fluxes of particulate-related components (e.g., metals, some nutrients, and organic matter) might be a driving force of fueling the flourishing hydrothermal organisms and metal accumulation on mollusks.

4.4 *Implications for the hydrothermal plume*

Based on current information, distinctive characteristics were observed in the hydrothermal plume from general deep oceans. First, the Fe- and Mn-rich particles, such as Fe- and Mn-sulfides (Sun et al., 2014) in the hydrothermal effluent plume (Pavia et al., 2019) can disperse with the plume over a large spatial range (Siegel et al., 2008; Wang et al., 2012; Estapa et al., 2015). During this dispersal, particle-reactive metals such as Th, Pb, Po, were absorbed on these particles and aggregation into POC by binding with DOC (Toner et al., 2009) over the timescale of days- to a hundred of days (Feely et al., 1990; Boisson et al., 2001; Owens et al., 2015; Yang et al., 2016). Then, metal-rich particles settled down to seafloor along the plume passage over the timescale of days to tens of days (this study and Yang et al. (2016)), possible causing the metal accumulation in benthic organisms. Inorganic particles acted simultaneously as the ballast and the settling of organic components induced. Finally, the enhanced sedimentation of particulate organic matter might deliver abundant metals to benthic ecosystems. The previous study suggested that POC source largely determines the activities of sediment-mixing benthos (Smith and Rabouille, 2002), the higher POC flux to the seafloor, the much deeper of the mixed layer in sediments (Smith et al., 2008). Thus, the enhanced organic matter flux may result in

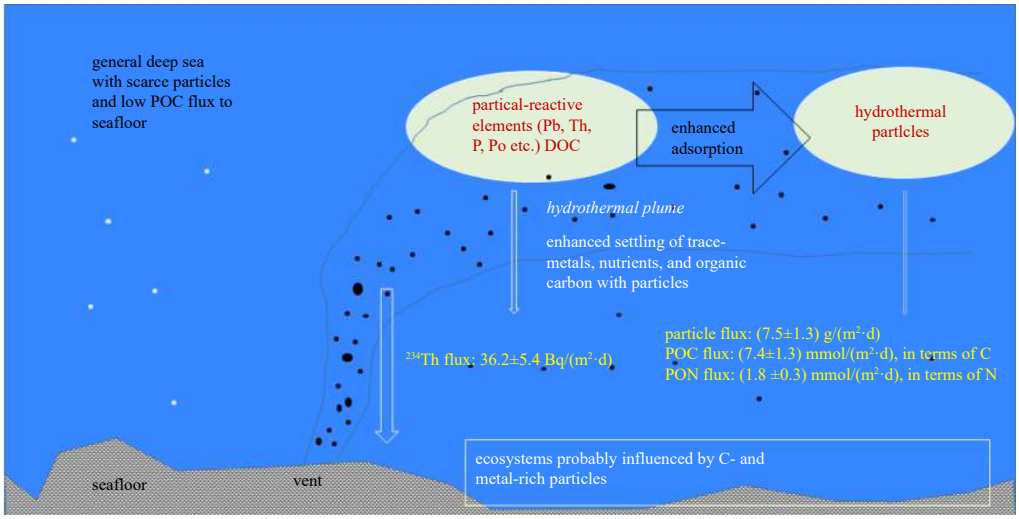

Fig. 6. The particle-reactive elements adsorption, sinking and its environmental implications in the hydrothermal plume.

different sediment environments below the hydrothermal plumes comparing with general deep oceans.

As shown in Fig. 6, all these unusual characteristics probably develop a special environment region in deep oceans. Although this study have a glimpse of the hydrothermal effluent plume, it is still a veiled system. As reviewed by Santos et al. (2018), the development of new tools and technologies would help the understanding of deep-sea mining-related environmental assessment. This study indicated that radioactive nuclides, e.g., Th isotopes (Owens et al., 2015; Yang et al., 2016; Pavia et al., 2019), would be effective tool for evaluating particle and metal cycling in hydrothermal effluent plumes.

5 Concluding remarks

Unusual deficits of radioactive ^{234}Th with respect to its parent ^{238}U allow us to examine the kinetics of particle-reactive metals in the hydrothermal plume over the SWIR. Unlike general deep oceans, the hydrothermal plume showed enhanced particle-reactive metal adsorption and sinking. Both adsorption and sinking constants of ^{234}Th suggested that particle-reactive elements (e.g., Th, Pb, Po, P) could be effectively removed by hydrothermal particles from the plumes over the timescales of days to tens of days, and these elements were transported to bottom water and seafloor, which would increase the metal accumulation in benthic organisms. In addition, hydrothermal particles have the capability to aggregate DOC and deliver it efficiently to sediments to sustain the benthos. These results indicated that the hydrothermal plume, as a typical environment region, has its own characteristics different from general deep oceans, and thus intensive and extensive investigations were required before deep-sea mining activities.

Acknowlegements

We appreciate the reviewers for their constructive comments and the help from the crew of R/V *Dayang I* during sampling.

References

Anand S S, Rengarajan R, Sarma V V S S. 2018. ^{234}Th-based carbon export flux along the Indian GEOTRACES GI02 section in the Arabian Sea and the Indian Ocean. Global Biogeochemical Cycles, 32(3): 417–436, doi: 10.1002/2017GB005847

Bacon M P, Rutgers van der Loeff M M. 1989. Removal of thorium-234 by scavenging in the bottom nepheloid layer of the ocean. Earth and Planetary Science Letters, 92(2): 157–164, doi: 10.1016/0012-821X(89)90043-5

Bacon M P, Spencer D W, Brewer P G. 1976. ^{210}Pb/^{226}Ra and ^{210}Po/^{210}Pb disequilibria in seawater and suspended particulate matter. Earth and Planetary Science Letters, 32(2): 277–296, doi: 10.1016/0012-821X(76)90068-6

Beaulieu S E, Mullineaux L S, Adams D K, et al. 2009. Comparison of a sediment trap and plankton pump for time-series sampling of larvae near deep-sea hydrothermal vents. Limnology and Oceanography, 7(3): 235–248, doi: 10.4319/lom.2009.7.235

Benitez-Nelson C R, Buesseler K O, Karl D M, et al. 2001a. A time-series study of particulate matter export in the North Pacific Subtropical Gyre based on ^{234}Th: ^{238}U disequilibrium. Deep-Sea Research Part I: Oceanographic Research Papers, 48(12): 2595–2611, doi: 10.1016/S0967-0637(01)00032-2

Benitez-Nelson C R, Buesseler K O, Rutgers van der Loeff M, et al. 2001b. Testing a new small-volume technique for determining ^{234}Th in seawater. Journal of Radioanalytical and Nuclear Chemistry, 248(3): 795–799, doi: 10.1023/A:1010621618652

Bi Qianqian, Du Jinzhou, Wu Ying, et al. 2013. Particulate organic carbon export flux by ^{234}Th/^{238}U disequilibrium in the continental slope of the East China Sea. Acta Oceanologica Sinica, 32(10): 67–73, doi: 10.1007/s13131-013-0303-7

Boisson F, Miquel J C, Cotret O, et al. 2001. ^{210}Po and ^{210}Pb cycling in a hydrothermal vent zone in the coastal Aegean Sea. Science of the Total Environment, 281(1–3): 111–119, doi: 10.1016/S0048-9697(01)00840-3

Buesseler K O, Bacon M P, Cochran J K, et al. 1992. Carbon and nitrogen export during the JGOFS North Atlantic bloom experiment estimated from ^{234}Th: ^{238}U disequilibria. Deep-Sea Research Part A: Oceanographic Research Papers, 39(7–8): 1115–1137, doi: 10.1016/0198-0149(92)90060-7

Buesseler K O, Pike S, Maiti K, et al. 2009. Thorium-234 as a tracer of spatial, temporal and vertical variability in particle flux in the North Pacific. Deep-Sea Research Part I: Oceanographic Research Papers, 56(7): 1143–1167, doi: 10.1016/j.dsr.2009.04.001

Cai Pinghe, Chen Weifang, Dai Minhan, et al. 2008. A high-resolution study of particle export in the southern South China Sea based on ^{234}Th: ^{238}U disequilibrium. Journal of Geophysical Research, 113(C4): C04019, doi: 10.1029/2007JC004268

Chakraborty P, Sander S G, Jayachandran S, et al. 2014. Fate of copper complexes in hydrothermally altered deep-sea sediments from the Central Indian Ocean Basin. Environmental Pollution, 194: 138–144, doi: 10.1016/j.envpol.2014.07.012

Charette M A, Moran S B, Bishop J K B. 1999. ^{234}Th as a tracer of particulate organic carbon export in the subarctic northeast Pacific Ocean. Deep Sea Research Part II: Topical Studies in Oceanography, 46(11–12): 2833–2861, doi: 10.1016/S0967-0645(99)00085-5

Coppola L, Roy-Barman M, Mulsow S, et al. 2005. Low particulate organic carbon export in the frontal zone of the Southern Ocean (Indian sector) revealed by ^{234}Th. Deep-Sea Research Part I: Oceanographic Research Papers, 52(1): 51–68, doi: 10.1016/j.dsr.2004.07.020

Coppola L, Roy-Barman M, Wassmann P, et al. 2002. Calibration of sediment traps and particulate organic carbon export using ^{234}Th in the Barents Sea. Marine Chemistry, 80(1): 11–26, doi: 10.1016/S0304-4203(02)00071-3

Estapa M L, Breier J A, German C R. 2015. Particle dynamics in the rising plume at Piccard Hydrothermal Field, Mid-Cayman Rise. Geochemistry, Geophysics, Geosystems, 16(8): 2762–2774, doi: 10.1002/2015GC005831

Feely R A, Massoth G J, Baker E T, et al. 1990. The effect of hydrothermal processes on midwater phosphorus distributions in the northeast Pacific. Earth and Planetary Science Letters, 96(3–4): 305–318, doi: 10.1016/0012-821X(90)90009-M

German C R, Colley S, Palmer M R, et al. 2002. Hydrothermal plume-particle fluxes at 13°N on the East Pacific Rise. Deep-Sea Research Part I: Oceanographic Research Papers, 49(11): 1921–1940, doi: 10.1016/S0967-0637(02)00086-9

German C R, Legendre L L, Sander S G, et al. 2015. Hydrothermal Fe cycling and deep ocean organic carbon scavenging: model-based evidence for significant POC supply to seafloor sediments. Earth and Planetary Science Letters, 419: 143–153, doi: 10.1016/j.epsl.2015.03.012

Guo Laodong, Chen Min, Gueguen C. 2002. Control of Pa/Th ratio by particulate chemical composition in the ocean. Geophysical Research Letters, 29(20): 1961, doi: 10.1029/2002GL015666

Hayes C T, Anderson R F, Fleisher M Q, et al. 2015. Intensity of Th and Pa scavenging partitioned by particle chemistry in the North Atlantic Ocean. Marine Chemistry, 170: 49–60, doi: 10.1016/j.marchem.2015.01.006

Huang Dekun, Du Jinzhou, Moore W S, et al. 2013. Particle dynamics of the Changjiang Estuary and adjacent coastal region determined by natural particle-reactive radionuclides (^{7}Be, ^{210}Pb, and ^{234}Th). Journal of Geophysical Research, 118(4): 1736–1748, doi: 10.1002/jgrc.20148

Hung C C, Gong G C. 2010. POC/^{234}Th ratios in particles collected in sediment traps in the northern South China Sea. Estuarine, Coastal and Shelf Science, 88(3): 303–310, doi: 10.1016/j.ecss.2010.04.008

Hung C C, Gong G C, Santschi P H. 2012. ^{234}Th in different size classes of sediment trap collected particles from the Northwestern Pacific Ocean. Geochimica et Cosmochimica Acta, 91:

60–74, doi: 10.1016/j.gca.2012.05.017
Ingebritsen S E, Evans W C. 2019. Potential for increased hydrothermal arsenic flux during volcanic unrest: implications for California water supply. Applied Geochemistry, 108: 104384, doi: 10.1016/j.apgeochem.2019.104384
Kádár E, Costa V, Segonzac M. 2007. Trophic influences of metal accumulation in natural pollution laboratories at deep-sea hydrothermal vents of the Mid-Atlantic Ridge. Science of the Total Environment, 373(2–3): 464–472, doi: 10.1016/j.scitotenv.2006.12.022
Kadko D, Feely R, Massoth G. 1994. Scavenging of ^{234}Th and phosphorus removal from the hydrothermal effluent plume over the North Cleft segment of the Juan de Fuca Ridge. Journal of Geophysical Research, 99(B3): 5017–5024, doi: 10.1029/93JB02952
Liao Shili, Tao Chunhui, Li Huaiming, et al. 2017. Use of portable X-ray fluorescence in the analysis of surficial sediments in the exploration of hydrothermal vents on the Southwest Indian Ridge. Acta Oceanologica Sinica, 36(7): 66–76, doi: 10.1007/s13131-017-1085-0
Lin Peng, Chen Min, Guo Laodong. 2012. Speciation and transformation of phosphorus and its mixing behavior in the Bay of St. Louis estuary in the northern Gulf of Mexico. Geochimica et Cosmochimica Acta, 87: 283–298, doi: 10.1016/j.gca.2012.03.040
Lin Peng, Guo Laodong, Chen Min. 2014. Adsorption and fractionation of thorium and protactinium on nanoparticles in seawater. Marine Chemistry, 162: 50–59, doi: 10.1016/j.marchem.2014.03.004
Lozano-Bilbao E, Gutiérrez á J, Hardisson A, et al. 2018. Influence of the submarine volcanic eruption off El Hierro (Canary Islands) on the mesopelagic cephalopod's metal content. Marine Pollution Bulletin, 129(2): 474–479, doi: 10.1016/j.marpolbul.2017.10.017
Ma Hao, Zeng Zhi, Yu Wen, et al. 2011. ^{234}Th/^{238}U disequilibrium and particulate organic carbon export in the northwestern South China Sea. Acta Oceanologica Sinica, 30(3): 55–62, doi: 10.1007/s13131-011-0119-2
Ma Haoyang, Yang Weifeng, Zhang Lihao, et al. 2017. Utilizing ^{210}Po deficit to constrain particle dynamics in mesopelagic water, western South China Sea. Geochemistry, Geophysics, Geosystems, 18(4): 1594–1607, doi: 10.1002/2017GC006899
Owens S A, Buesseler K O, Sims K W W. 2011. Re-evaluating the ^{238}U-salinity relationship in seawater: Implications for the ^{238}U-^{234}Th disequilibrium method. Marine Chemistry, 127(1–4): 31–39, doi: 10.1016/j.marchem.2011.07.005
Owens S A, Pike S, Buesseler K O. 2015. Thorium-234 as a tracer of particle dynamics and upper ocean export in the Atlantic Ocean. Deep-Sea Research Part II: Topical Studies in Oceanography, 116: 42–59, doi: 10.1016/j.dsr2.2014.11.010
Pancaldi F, Galván-Magaña F, González-Armas R, et al. 2019. Mercury and selenium in the filter–feeding whale shark (*Rhincodon typus*) from two areas of the Gulf of California, Mexico. Marine Pollution Bulletin, 146: 955–961, doi: 10.1016/j.marpolbul.2019.07.017
Pavia F J, Anderson R F, Black E E, et al. 2019. Timescales of hydrothermal scavenging in the South Pacific Ocean from ^{234}Th, ^{230}Th, and ^{228}Th. Earth and Planetary Science Letters, 506: 146–156, doi: 10.1016/j.epsl.2018.10.038
Peng S H, Hung J J, Hwang J S. 2011. Bioaccumulation of trace metals in the submarine hydrothermal vent crab *Xenograpsus testudinatus* off Kueishan Island, Taiwan. Marine Pollution Bulletin, 63(5–12): 396–401, doi: 10.1016/j.marpolbul.2011.05.013
Ran Lihua, Chen Jianfang, Wiesner M G, et al. 2015. Variability in the abundance and species composition of diatoms in sinking particles in the northern South China Sea: Results from time-series moored sediment traps. Deep-Sea Research Part II: Topical Studies in Oceanography, 122: 15–24, doi: 10.1016/j.dsr2.2015.07.004
Ray D, Banerjee R, Mazumder A, et al. 2018. Mineralogical and geochemical variation in hydrothermal sulfides from Vienna Woods field, Manus Basin, Papua New Guinea: constraints on their evolution. Acta Oceanologica sinica, 37(4): 22–33, doi: 10.1007/s13131-018-1194-4
Rixen T, Gaye B, Emeis K C. 2019. The monsoon, carbon fluxes, and the organic carbon pump in the northern Indian Ocean. Progress in Oceanography, 175: 24–39, doi: 10.1016/j.pocean.2019.03.001
Roca-Martí M, Puigcorbé V, Iversen M H, et al. 2017. High particulate organic carbon export during the decline of a vast diatom bloom in the Atlantic sector of the Southern Ocean. Deep-Sea Research Part II: Topical Studies in Oceanography, 138: 102–115, doi: 10.1016/j.dsr2.2015.12.007
Rutgers van der Loeff M M, Buesseler K, Bathmann U, et al. 2002. Comparison of carbon and opal export rates between summer and spring bloom periods in the region of the Antarctic Polar Front, SE Atlantic. Deep-Sea Research Part II: Topical Studies in Oceanography, 49(18): 3849–3869, doi: 10.1016/S0967-0645(02)00114-5
Santos M M, Jorge P A S, Coimbra J, et al. 2018. The *last frontier*: coupling technological developments with scientific challenges to improve hazard assessment of deep-sea mining. Science of the Total Environment, 627: 1505–1514, doi: 10.1016/j.scitotenv.2018.01.221
Schmidt S. 2006. Impact of the Mediterranean outflow water on particle dynamics in intermediate waters of the Northeast Atlantic, as revealed by ^{234}Th and ^{228}Th. Marine Chemistry, 100(3–4): 289–298, doi: 10.1016/j.marchem.2005.10.017
Shih Y Y, Lin H H, Li Dewang, et al. 2019. Elevated carbon flux in deep waters of the South China Sea. Scientific Reports, 9(1): 1496, doi: 10.1038/s41598-018-37726-w
Siegel D A, Fields E, Buesseler K O. 2008. A bottom-up view of the biological pump: modeling source funnels above ocean sediment traps. Deep-Sea Research Part I: Oceanographic Research Papers, 55(1): 108–127, doi: 10.1016/j.dsr.2007.10.006
Smith C R, De Leo F C, Bernardino A F, et al. 2008. Abyssal food limitation, ecosystem structure and climate change. Trends in Ecology & Evolution, 23(9): 518–528, doi: 10.1016/j.tree.2008.05.002
Smith C R, Rabouille C. 2002. What controls the mixed-layer depth in deep-sea sediments? The importance of POC flux. Limnology and Oceanography, 47(2): 418–426, doi: 10.4319/lo.2002.47.2.0418
Sun Xiaoxia. 2011. Study on the suspended particulate minerals in the water column in the Eastern Equatorial Pacific Ocean and hydrothermal active areas in the Southwest Indian Ocean (in Chinese) [dissertation]. Qingdao: Ocean University of China
Sun Xiaoxia, Yang Zuosheng, Fan Dejiang, et al. 2014. Suspended zinc sulfide particles in the Southwest Indian Ridge area and their relationship with hydrothermal activity. Chinese Science Bulletin, 59(9): 913–923, doi: 10.1007/s11434-014-0118-8
Tao Chunhui, Lin Jian, Guo Shiqin, et al. 2012. First active hydrothermal vents on an ultraslow-spreading center: Southwest Indian Ridge. Geology, 40(1): 47–50, doi: 10.1130/G32389.1
Toner B M, Fakra S C, Manganini S J, et al. 2009. Preservation of iron(II) by carbon-rich matrices in a hydrothermal plume. Nature Geoscience, 2(3): 197–201, doi: 10.1038/ngeo433
Turnewitsch R, Reyss J L, Nycander J, et al. 2008. Internal tides and sediment dynamics in the deep sea—Evidence from radioactive ^{234}Th/^{238}U disequilibria. Deep-Sea Research Part I: Oceanographic Research Papers, 55(12): 1727–1747, doi: 10.1016/j.dsr.2008.07.008
Wang Hu, Yang Qunhui, Ji Fuwu, et al. 2012. The geochemical characteristics and Fe(II) oxidation kinetics of hydrothermal plumes at the Southwest Indian Ridge. Marine Chemistry, 134–135: 29–35, doi: 10.1016/j.marchem.2012.02.009
Yang Weifeng, Chen Min, Cao Jianping, et al. 2009. Influence of particle composition on thorium scavenging in the marginal China Seas. Acta Oceanologica Sinica, 28(2): 45–53, doi: 10.3969/j.issn.0253-505X.2009.02.005
Yang Weifeng, Chen Min, Zheng Minfang, et al. 2015a. Influence of a decaying cyclonic eddy on biogenic silica and particulate organic carbon in the Tropical South China Sea based on ^{234}Th-^{238}U disequilibrium. PLoS One, 10(8): e0136948, doi: 10.1371/

journal.pone.0136948

Yang Weifeng, Guo Laodong, Chuang C Y, et al. 2013. Adsorption characteristics of ^{210}Pb, ^{210}Po and ^{7}Be onto micro-particle surfaces and the effects of macromolecular organic compounds. Geochimica et Cosmochimica Acta, 107: 47–64, doi: 10.1016/j.gca.2012.12.039

Yang Weifeng, Guo Laodong, Chuang C Y, et al. 2015b. Influence of organic matter on the adsorption of ^{210}Pb, ^{210}Po and ^{7}Be and their fractionation on nanoparticles in seawater. Earth and Planetary Science Letters, 423: 193–201, doi: 10.1016/j.epsl.2015.05.007

Yang Weifeng, Zhang Xinxing, Chen Min, et al. 2016. Unusually low ^{234}Th in a hydrothermal effluent plume over the Southwest Indian Ridge. Geochemistry, Geophysics, Geosystems, 17(9): 3815–3824, doi: 10.1002/2016GC006580

Zhang Jingjing, Li Hongliang, Xuan Jiliang, et al. 2019. Enhancement of mesopelagic sinking particle fluxes due to upwelling, aerosol deposition, and monsoonal influences in the Northwestern South China Sea. Journal of Geophysical Research, 124(1): 99–112, doi: 10.1029/2018JC014704